On Curve Negotiation: From Driver Support to Automation

Paolo Bosetti, Mauro Da Lio, *Member, IEEE*, and Andrea Saroldi

***Abstract*—This paper describes a curve negotiation "behavior" that can be used—within subsumption architectures—to produce artificial agents with the ability to negotiate curves in a human-like way. This may be used to implement functions spanning different levels of automation, from assistance (curve warning) to automated (curve speed control). This paper gives the following: 1) a summary of related works and of the subsumption architecture conceptual framework; 2) a detailed description of the function within this framework; 3) experimental data for validation and tuning derived from user tests; 4) guidelines on integration of the function within advanced driver assistance systems with different automation levels, with examples; and 5) a comparison with experimental data of the human curve speed choice models in the state of the art.**

***Index Terms*—Advanced driver assistance systems (ADAS), anticipatory longitudinal control, co-driver, curve speed, driver modeling, optimal control (OC).**

I. Introduction

THIS paper is focused on the anticipatory longitudinal speed control that ought to be used to properly drive on curvy roads in a way similar to human drivers.

A *curve behavior* is developed, which, in the conceptual framework of subsumption control architectures, can be easily integrated into *co-driving agents* fulfilling different levels of automation. For example, it may be used in an assistive fashion to mirror the human driver, for understanding his/her intentions, and in particular whether she/he may be approaching curves in an unusual way (possibly incorrect and dangerous). At the other extreme, for driving automation, it may be used to produce longitudinal controls that adapt to the lane curvature.

A. Subsumption Architectures

The idea of structuring complex behaviors by means of layered control architectures dates back to mid 1980s [1]. Although it has been originally proposed for robots, evidence was then found that the brain of vertebrates is structured hierarchically in a similar way [2]. In subsumption architectures, every layer of the hierarchy achieves newer and more complex competences by subsuming the behaviors of the layers underneath it.

Within this conceptual framework, the curve behavior hereafter described shall be considered as an intermediate layer for more complex applications. By changing the way in which the function is used (i.e., subsumed), applications spanning different levels of automation will be demonstrated.

Consistent with this approach, the function itself is produced by subsuming elementary motor units, called *motor primitives*.

B. Related Works

A number of studies deal with the concept of *safe speed in curves*, or—which is equivalent—lateral acceleration. It has been noted that, for cars driving along horizontal roads, ordinary drivers (i.e., not trained race drivers) use longitudinal and lateral accelerations that belong to a subset of the tire friction ellipse, represented in the g–g diagram with a shape similar to a rhomb or a mushroom or a cross [3]–[7].

Some authors directly derive the curve speed from the tire friction ellipse, by adopting proper safety margins, and often considering additional factors, such as road slope, banking, etc. [8]–[12].

However, other studies have shown that the *human choice of speed in curves* follows criteria other than merely the friction limits [7], [13]–[15]. In particular, the accepted lateral acceleration is not constant (as it would be if it were a fraction of the friction limit) but decreases with increasing speed [7], [14], [15]. Winsum *et al.* [16] and Reymond *et al.* [17] explain this observation with the existence of human control strategies aimed at achieving a robust lateral control. More precisely, the speed is adapted to the curvature primarily to keep the lateral error bounded, given uncertainties in the estimated road curvature and noise in the (human) steering control. With this explanation, the width of the road (which influences the accepted bounds) is also recognized as a contributing factor [18], [19]. To support the sensory-motor interpretation for the speed choice, it must be mentioned that similar strategies have been discovered for hand-tracing [20] and for walking [21] and explained in terms of the *minimum variance principle* [22].

In the domain of *preventive safety applications*, curve warning applications have been presented by several authors.

In [8] a modified ISA (Intelligent Speed Adaptation) system is described, in which safe speed is computed, per road stretches, according to several types of hazards, including curves (based on friction ellipse and superelevation). Transition zones, harmonizing the speed profile, are introduced between road stretches that would otherwise produce discontinuous

Manuscript received September 7, 2014; revised January 8, 2015; accepted January 14, 2015. This work was supported in part by the European Commission under Grants FP7 246587 (interactIVe) and FP7 610428 (adaptIVe). The Associate Editor for this paper was M. Brackstone.

P. Bosetti and M. Da Lio are with the Department of Industrial Engineering, University of Trento, 38123 Trento, Italy (e-mail: paolo.bosetti@unitn.it; mauro.dalio@unitn.it).

A. Saroldi is with Centro Ricerche Fiat, 10043 Orbassano, Italy (e-mail: andrea.saroldi@crf.it).

Color versions of one or more of the figures in this paper are available online at http://ieeexplore.ieee.org.

Digital Object Identifier 10.1109/TITS.2015.2395819

recommended speed. In [9] an anticipatory ISA system is introduced: the system *recommends the acceleration* necessary to match the speed of the next stretch, and issues warnings if it exceeds given thresholds. The maneuver to adapt the speed to the next stretch is simplified in two phases: a first phase—spanning the driver's time of reaction—in which the vehicle moves at constant speed, and a second phase with uniform deceleration (this deceleration is used for driver assistance). A similar approach has been previously adopted in [23] for the generation of curve speed warnings based on required vehicle deceleration.

In [10] and [11] a maximum speed envelope is defined over road stretches, using a fraction of the friction ellipse, by combining cornering with acceleration and braking. Given the current acceleration, speed and a short forecast horizon, the *probability of trespassing the speed envelope* is evaluated and used to raise warnings.

In [24]–[26] a *reference maneuver* is computed according to an optimal control scheme to meet multiple objectives, among which curve negotiation. It represents how a human would correctly and optimally drive (e.g., it complies with the speed-dependent acceleration willingness envelope). Longitudinal and lateral controls are simultaneously produced within a receding horizon scheme. The reference maneuver is used as a *gold standard* to detect driver incorrect behavior and issue warnings.

For applications involving *automated driving*, the longitudinal control (or at least a target speed profile) is necessary. For example, a reference maneuver like the above might be, in principle, used for controlling the vehicle.

In [12] a *sliding mode controller* is described to follow a desired speed profile. The latter is computed in a way similar to [10] and [11], i.e., from the friction ellipse and the road geometry, assuming that the allowed fraction of the friction ellipse is entirely mobilized. The authors note that this system shows some jerkiness, caused by the purely geometric method of computation of the target speed profile, which is coupled to a precise controller. An alternative PID controller was tested, resulting smoother, but less precise in following the target speed. Thus, in [27] a strategy switching between two PID controllers is proposed: a more vigorous controller is used when the speed exceeds the safe speed by more than 15% and it is used for decelerating to safe speed. A second controller, with reduced proportional gain, is instead used for tracking the safe speed in its proximity. Lastly, if the speed is below 85% of the safe speed, the control is yield back to the human driver.

The integration of a curve speed control function with an ACC system is presented in [28]. The system first fits a two-parameters function onto the entry and exit speed profiles observed for human drivers in manual operation. Then, it uses the fitted function in automated driving to produce the target speed profile. The speed for the curve supersedes the set-point of the traditional ACC when it is slower. A PI controller is used for speed tracking. However, in this implementation the speed at the curve apex is a function of the entrance speed (which is the previous ACC speed set-point). Thus, while the system reduces the speed in curves, it does not always achieve the same minimum speed, which should instead be the case according to the sensory-motor strategies above mentioned.

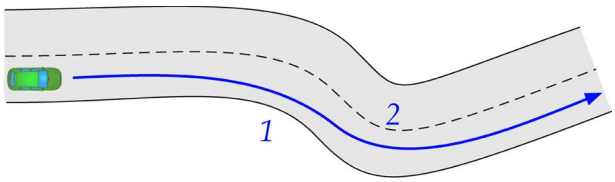

Fig. 1. Scenario of a curvy road.

II. Maneuvering for Curves

A. Problem Definition

Let us consider a vehicle traveling on a curvy road as schematically shown in Fig. 1. The problem is to find a *reference maneuver* that negotiates the curves with speed and acceleration levels assumed as acceptable for humans.

Such problem can be split in two steps: first, to define which is the speed that must be obeyed inside the curve (Section II-B); and second, to define a deceleration policy that achieves that speed (Section II-C–E).

B. Velocity–Acceleration–Curvature Correlation in Humans

As pointed out in Section I-B, many approaches used to restrict the lateral acceleration (a_{lat}) to a fraction of the tire cornering limit (μg) in order to find the limit speed in curves:

$$\frac{v^2}{r} = a_{\mathrm{lat}} \leq k_s \mu g, \tag{1}$$

where v denotes the speed and r the path radius. The implicit idea behind this is that the human goal, when driving, is to maintain a suitable safety margin k_s with respect to tire friction limits.

However, other studies have shown that the primary innate human goal is probably different. In fact, inverse correlation between curvature and speed has been explained as a strategy for minimizing the effects of steering errors [16], [17], or for achieving robust control in the more general domain of human sensory-motor strategies [22] (see [7] for further discussion).

Levison *et al.* [15, p. 58] give the following formula for predicting the accepted lateral acceleration in curved paths:

$$a_{\mathrm{lat}} = \frac{k^2}{v^2}, \tag{2}$$

which is based on data analysis of three selected curves of the Battelle on-road study—with $k = 36\ \mathrm{m}^{3/2}/\mathrm{s}^2$ representing 50 percentiles of car drivers and $k = 42\ \mathrm{m}^{3/2}/\mathrm{s}^2$ 85 percentiles.

On the other hand, inverse correlation between speed and curvature—known to be a general feature of human movement—is modeled by the *two-thirds power law*[1] [20]:

$$a_{\mathrm{lat}} = \frac{\alpha^3}{v} \tag{3}$$

Authors found the two-thirds law to be a better fit than (2) for the data logged in the user-test of the "interactIVe" project, which was a mixed scenario with both urban, extra-urban

[1]The name comes from the acceleration-curvature function.

roads, and motorways [7]. Authors reckoned $\alpha = 3.7\ \mathrm{m}^{2/3}/\mathrm{s}$ to represent 99.9 percentiles of the observed data, $\alpha = 3.6\ \mathrm{m}^{2/3}/\mathrm{s}$ to represent the 95 percentile driver, and $\alpha = 3.34\ \mathrm{m}^{2/3}/\mathrm{s}$ to represent the median driver. These figures hold for urban and extra-urban roads. Motorways tend to be driven at constant speed and make an exception with larger accepted accelerations, probably because of their much greater width.

In addition, Authors found that an even better fit may be obtained with the following:

$$a_{\mathrm{lat}} = \frac{a_0}{\sqrt{\left(1 - \frac{v^2}{v_0^2}\right)^2 + 2\frac{v^2}{v_0^2}}}, \tag{4}$$

which was named "modified Levison's criterion" since it is asymptotic to (2), but better models the saturation of lateral acceleration at low speed.

The 99.9 percentile of the observed data is described by $a_0 = 5.22\ \mathrm{m/s}^2$ and $v_0 = 14.84\ \mathrm{m/s}$. Other percentiles can be obtained by changing a_0 as follows: $a_0 = 4.81\ \mathrm{m/s}^2$ for 95 percentiles and $a_0 = 4.20\ \mathrm{m/s}^2$ for the median driver.

Lastly, Reymond's lateral acceleration margin model [17] produces the following formula:

$$a_{\mathrm{lat}} = k_1 - k_2 v^2 \tag{5}$$

The coefficients, estimated for seven young drivers on a test track, have the following mean value for normal driving: $k_1 = 7.64\ \mathrm{m/s}^2$ and $k_2 = 6.32 \times 10^{-3}\ \mathrm{m}^{-1}$.

It must be noted that, strictly speaking, all these fitting curves hold for the context of the experiment, in which data have been collected: road types (in particular lane width as pointed out in Section I-B), users culture, and vehicle type (which was always a car). Extension to other situations—in particular to other types of vehicles and different lane widths—must be considered with care and may require further data.

Finally, by substituting $a_{\mathrm{lat}} = v^2/r$ in (3), (4), or (5), one gets the conditions that the speed must satisfy, given as a function of the trajectory curvature (κ):

- Two-Thirds law:

$$v \leq \alpha \kappa^{-\frac{1}{3}} \tag{6}$$

- Modified Levison:

$$v \leq v_0 \sqrt{\sqrt{\frac{{a_0}^2}{\kappa^2 {v_0}^4} + \frac{1}{4}} - \frac{1}{2}} \tag{7}$$

- Reymond:

$$v \leq \sqrt{\frac{k_1}{(\kappa + k_2)}}. \tag{8}$$

A comparison between these different formulas is given in Section V. Note that the different formulas can prove difficult to discriminate if the radius of the curves spans a restricted range. Extrapolation of the fitting equations outside the radius range where they were fitted must also be considered carefully.

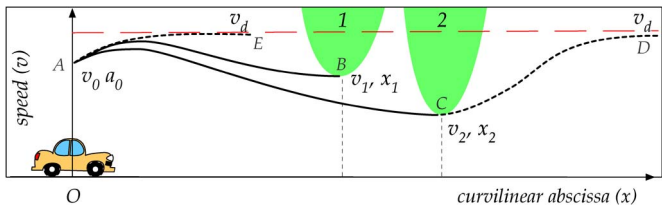

Fig. 2. Maneuver planning.

C. Optimal Longitudinal Control

We aim at defining a longitudinal control policy for traveling close to a desired speed (v_d), in full comfort and without violating curvature–speed constraints. Fig. 2 illustrates such objectives.

This quite complex desired *curve behavior* may be formulated as an optimal control problem, not only because it is as a convenient mathematical tool for such problem category, but mainly because of the consolidated opinion—in cognitive and behavioral sciences—that optimal control successfully models flexible/optimized human sensory-motor strategies [29]–[31]. Consequently, the task described in Fig. 2 can be expressed mathematically as follows.

First, let us consider a third order dynamic system modeling the longitudinal kinematics:

$$\dot{s}(t) = v(t),\ \dot{v}(t) = a(t),\ \dot{a}(t) = j(t) \tag{9}$$

where j is the control input and s, v, and a are the states, respectively standing for the longitudinal traveled distance, longitudinal velocity, and longitudinal acceleration. The reason supporting this choice is that the aim is to develop motor plans at an abstract, i.e., kinematic, level. Note that the idea of planning at the kinematic—rather than dynamic—level is also supported by some works dealing with robust optimal stochastic human motor control [32].

We aim at finding the particular input $j(t)$, which minimizes the following cost functional J, with free final time T:

$$\underset{j(\cdot),T}{\textsc{Minimize}} \quad J \tag{10}$$

where:

$$J\left(j(\cdot), T\right) = \int_0^T w_T + j(t)^2\, \mathrm{d}t \tag{11}$$

subject to:

1) the initial conditions:

$$s(0) = 0,\ v(0) = v_0,\ a(0) = a_0; \tag{12}$$

2) the final conditions (the aimed state):

$$s(T) = \text{free},\ v(T) = v_d,\ a(T) = 0; \tag{13}$$

3) the velocity–curvature constrains, e.g., one of (6) or (7) or (8);
4) and the model equations (9).

Note that (11) is a trade-off between minimum time, modeled by the integral of weight w_T (which, being equal to Tw_T,

in turn implies the minimization of T), and minimum input energy, modeled by the integral of the square jerk $j(t)^2$. As such, it captures the competition between speed and accuracy inherent in any human movement: in fact, noise of human motion is proportional to the driving signal, and thus minimizing jerk also means minimizing the energy of the input noise, which approximates robust control (see also [22] and Section I-B).

D. Motor Primitives

The optimal control problem could be solved as a whole, producing a monolithic behavior such as A–D (Fig. 2), as was done in [24]–[26].

However, the problem may be tackled in a different way, by breaking it into simpler sub-problems that represent more basic motor tasks. This latter approach is here presented because of:

- *Consistency with bio-inspired hierarchical control architectures*: tasks/subtasks resulting from problem breakdown, can be naturally accommodated into behavioral hierarchical architectures such as those believed to hold for humans and animals [2], [33], [34].
- *Meaning of subproblems*: tasks/subtasks can be clearly interpreted to serve specific subgoals, concurring to form the complex behavior.
- *Scalability*: new tasks and new goals can be added in an easier way, potentially achieving more and more complex functions [1].
- *Less computational complexity*: the tasks resulting from problem breakdown are simpler to solve: inequality constraints may be avoided, and closed-form solutions may be available. These latter improve computation speed and do not suffer from convergence issues—which are dangerous in safety critical, real-time operations.
- *Intelligent behavior*: subsumptive hierarchical architectures achieve flexible intelligent behaviors, for example by means of action selection mechanisms, which will be demonstrated below.

After these considerations, the behavior given in Fig. 2 may be decomposed in simpler sub-problems as follows:

- One is negotiating a curve, e.g., A–B or A–C.
- Another is achieving a desired speed, e.g., C–D or A–E.

These are the two types of motor tasks that will be used in the followings. Given that these motor tasks will not be further divided, these are named *curve motor primitives*. In the following, the two motor primitives will be firstly described and then it will be shown how they can be combined to obtain the desired higher-level behavior.

1) Curve Motor Primitives: Negotiating *one* curve, such as A–C or A–B, is a simpler optimal control problem. Given that we consider one curve at a time, there are no equivalents of (6)–(8), and (9)–(12) still hold. However, the final condition in (13) is replaced by:

$$s(T) = s_c,\ v(T) = v_c,\ a(T) = 0 \tag{14}$$

with v_c and s_c expressing the match with the minimum speed at the curve apex (e.g., $s_c = s_2$ and $v_c = v_2$ at curve 2). This problem may be solved in *closed form*, for example by means of Calculus of Variations and Pontryagin's principle.

The solution $s_c(t)$—with subscript c meaning "curve primitive"—is a 5-*th* order polynomial, i.e.:

$$s_c(t) = c_1 t + \frac{1}{2}c_2 t^2 + \frac{1}{6}c_3 t^3 + \frac{1}{24}c_4 t^4 + \frac{1}{120}c_5 t^5 \tag{15}$$

with:

$$\begin{aligned} c_1 &= v_0,\ c_2 = a_0 \\ c_3 &= -\frac{9a_0}{T} + \frac{60s_c}{T^3} - \frac{12(3v_0 + 2v_c)}{T^2} \\ c_4 &= \frac{36a_0}{T^2} - \frac{360s_c}{T^4} + \frac{24(8v_0 + 7v_c)}{T^3} \\ c_5 &= -\frac{60a_0}{T^3} + \frac{720s_c}{T^5} - \frac{360(v_0 + v_c)}{T^4}. \end{aligned} \tag{16}$$

With this notation, the coefficients c_i represent the i-*th* derivative at $t = 0$, i.e., initial velocity c_1, initial acceleration c_2, initial jerk c_3, initial snap c_4, and initial crackle c_5 (where the crackle does not depend on time), respectively.

The derivatives have the same structure:

$$\begin{aligned} v_c(t) &= c_1 + c_2 t + \frac{1}{2}c_3 t^2 + \frac{1}{6}c_4 t^3 + \frac{1}{24}c_5 t^4 \\ a_c(t) &= c_2 + c_3 t + \frac{1}{2}c_4 t^2 + \frac{1}{6}c_5 t^3 \end{aligned} \tag{17}$$

and, in particular, the optimal control is quadratic:

$$j_c(t) = c_3 + c_4 t + \frac{1}{2}c_5 t^2 \tag{18}$$

The time T is yet to be defined (note that (11) is with *free* final time). It can be found by substituting (18) into (11) and minimizing, which yields:

$$\begin{aligned} J_c = T w_T + \frac{9{a_0}^2}{T} + \frac{24a_0(3v_0 + 2v_c)}{T^2} + \\ + \frac{24\left(-5a_0 s_c + 8{v_0}^2 + 14v_0 v_c + 8{v_c}^2\right)}{T^3} + \\ - \frac{720s_c(v_0 + v_c)}{T^4} + \frac{720{s_c}^2}{T^5}. \end{aligned} \tag{19}$$

It has to be noted that, for $T \to \infty$, J_c is asymptotic to T ($J_c \sim T$). Conversely, for $T \to 0^+$, $J_c \sim T^{-5}$. Therefore, there is at least one minimum for $T > 0$.

By equating the derivative of J_c to zero, the following polynomial equation for the stationary points is obtained:

$$\begin{aligned} w_T T^6 - 9{a_0}^2 T^4 - 48a_0(3v_0 + 2v_c)T^3 + \\ - 72\left(-5a_0 s_c + 8{v_0}^2 + 14v_0 v_c + 8{v_c}^2\right)T^2 + \\ + 2880s_c(v_0 + v_c)T - 3600{s_c}^2 = 0. \end{aligned} \tag{20}$$

Inspection of the coefficients, based on Descarte's rule of signs, indicates that there may be either 1, 3 or 5 positive roots. Fig. 3 shows how the solutions may look like for 3 roots, respectively for negative (left) and positive initial acceleration (right).

The first root, curve 1, is a local minimum of J_c; curve 2 is a local maximum and curve 3 a local minimum again (it would not be difficult to demonstrate that, if the roots are distinct,

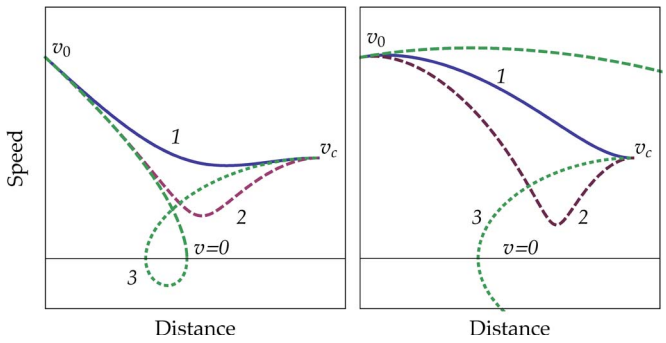

Fig. 3. Motor primitives for curve negotiation (see text).

odd roots are minima and even roots are maxima). Each local minimum represents, conceptually, a different strategy to meet the final conditions. Root 1 is the fastest strategy (because it is associated to the smallest T), whereas root 3 is another option which would dilute the control over a longer time. In the given example, curve 3 involves inversion of the direction of travel, but it may also happen that curve 3 looks similar to curve 2, with a minimum of speed and no reversing of the travel direction.

The first root is selected to produce a motor primitive with a consistent meaning—often the global minimum. It might happen that, for very large negative values of a_0, even this solution has a shape like curve 3. This means that stopping is unavoidable and, in this case, we retain the dashed part of the curve to the stop point ($v = 0$), albeit it would be more elegant to design a proper *stop primitive*.

Thus, in all cases the first positive root of the polynomial (20) is considered—and one can avoid comparing the cost function for all the roots. For computing the polynomial roots, the Jenkins–Traub algorithm [35] can be effectively used.

2) Free-Flow Motor Primitives: For this primitive, the final condition in (14) takes the form:

$$s(T) = \text{free},\ v(T) = v_d,\ a(T) = 0 \tag{21}$$

meaning that the target speed v_d may be reached at the most convenient point.

The solution of the optimal control problem is similar to (15), (17) and (18), but with different coefficients, which are:

$$\begin{aligned} c_1 &= v_0,\ c_2 = a_0 \\ c_3 &= \frac{6(v_d - v_0)}{T^2} - \frac{4a_0}{T} \\ c_4 &= \frac{6a_0}{T^2} + \frac{12(v_0 - v_d)}{T^3} \\ c_5 &= 0. \end{aligned} \tag{22}$$

Note that, since $c_5 = 0$, the degrees of polynomials are reduced by one respect to the previous case.

Following the same logic as in the previous section, the optimal primitive duration T is found by minimizing (11) with substitution of the new expression for the free-flow jerk profile $j_f(t)$. A new polynomial equation is thus obtained:

$$\begin{aligned} w_T T^4 - 4{a_0}^2 T^2 + 24 a_0 T(v_d - v_0) + \\ - 36(v_0 - v_d)^2 = 0. \end{aligned} \tag{23}$$

This may have 1 or 3 real positive roots, except if $v_d = v_0$ and $a_0 = 0$, in which case the solution is uniform speed ($c_3 = 0$ and $c_4 = 0$).

When there are 3 roots, the global minimum is always taken—i.e., this primitive is let to automatically switch to the global optimal strategy (unlike in the above). In the case of the type 3 curve (Fig. 3), the vehicle is performing a stop maneuver and only the part till the stop point is considered.

E. Curve Behavior

The two motor primitives can be combined into a higher-level behavior.

The subsumption mechanism here is *action-selection*. The idea is that the motor primitives are active in parallel. For instance, when the vehicle is at point O (Fig. 2), three motor primitives are simultaneously generated: one for the free flow goal and one for each of the two curves ahead. Then, the most appropriate primitive is selected *a posteriori*. This idea conforms to recent theories in cognitive behavioral sciences, such as the theory of *affordance competition* [36], which posits that multiple possible actions are produced simultaneously at the cortical level, and only one is selected at the basal ganglia [37].

The advantage of *a posteriori* selection is flexibility and adaptability to changing environments. For example, if curve 2 magically disappeared, or a new threat appears, the agent would/will more easily adapt to the changed context.

Selecting one action means choosing one of the control output generated by the (possibly many) primitives, i.e., the $j_c(t)$ of the proper curve, or the flee-flow $j_f(t)$.

Anyway, each action is represented by the three coefficients of $j(t)$. Among these, the most important is the initial jerk $j(0) = c_3$, which dominates the forthcoming dynamics. In a receding horizon framework, action selection may thus be carried out primarily by comparing values of $j(0)$.

In this paper, the selection process consists of simply choosing the maneuver corresponding to the smallest $j(0)$, i.e., A–C in Fig. 2. However, for more complex tasks, action selection may be more complex [37]. For example, if the behavior for passing a semaphore were to be included, it might be that $j(0)$ must be larger than a threshold in order to pass before the red light. Another example of a more complex selection was given in [38], where actions for combined longitudinal and lateral control had to be coordinated.

With the above explanations, the curve behavior may thus be defined with the following pseudo-code:

Require: $a_0, v_0, v_d, \kappa(s), w_T$
$j_f(s) \leftarrow$ FREEFLOW_PRIMITIVE(a_0, v_0, v_d, w_T)
$\mathbf{s}_c \leftarrow$ FIND_MAXIMA$(|\kappa(s)|)$ ▷ $\mathbf{s}_c$ is a list
$n \leftarrow$ LENGTH$(\mathbf{s}_c)$
for all $\mathbf{s}_c$ **do**
    $v_{c,i} \leftarrow$ CURVE_SPEED$(\kappa(s_{c,i}))$
    $j_{c,i}(s) \leftarrow$ CURVE_PRIMITIVE$(a_0, v_0, v_{c,i}, s_{c,i}, w_T)$
end for
$j^* \leftarrow \min\{j_f(0), j_{c,1}(0), \ldots, j_{c,n}(0)\}$
Select action with $j(0) = j^* \rightarrow c_1^*, c_2^*, \ldots, c_5^*$
return $c_1^*, c_2^*, \ldots, c_5^*$

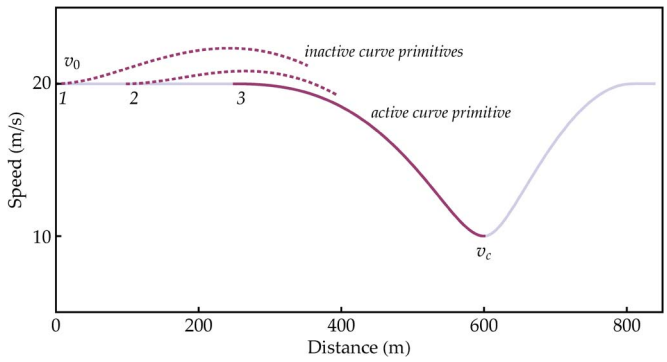

Fig. 4. Selection of primitives.

where a_0 and v_0 represent the initial state, $k(s)$ the environment (road curvature ahead), v_d and w_T the agent's goals, and c_i^* the coefficients of the active motor primitive. Finally, CURVE_SPEED calculates the minimum curve speed from the local curvature $\kappa(s_{c,i})$ from the Two-Thirds law, and CURVE_PRIMITIVE and FREEFLOW_PRIMITIVE are the result of case 1) and case 2) in the previous section, respectively.

As an example, the curve behavior for the case of a vehicle approaching a curve with initial speed equal to the desired speed ($v_d = v_0$) is considered and illustrated in Fig. 4. Far from the curve, e.g., in points 1 and 2, the curve primitive would produce an initial acceleration (because of the term w_T), as shown by the dotted curves. The selected action, is therefore free-flow ($v(t) = v_0 = v_d$), since $j_f(0) < j_c(0)$. However, as the vehicle comes closer to the curve, e.g., in point 3, the curve primitive no longer foresees initial acceleration. After point 3, the curve primitive is selected to decelerate until the curve apex. After this point, only the free-flow primitive exists—but now the speed is close to v_c, the desired speed is still v_d, and thus the free-flow primitive generates the post-curve speed-up. The point where the switching between primitives occurs (point 3) is influenced by w_T (the larger w_T, the later the switching). The minimum speed is also influenced by w_T, and thus v_c may not coincide with the curve minimum.

III. Experimental Data

The experimental data, collected during the user tests of the EU project "interactIVe" [39], are used for validation and system tuning.

The test loop, Fig. 5, follows the alphabetic order of letters *a* to *g*, then returns to *a*. It includes urban arterials (*a–b*), motorways (*c–d–e*) and extra-urban roads, with related links, roundabouts, ramps, and intersections (see also [7]).

The vehicle driven during the tests was a Lancia Delta, equipped with a rich set of sensors. The signals that are relevant for this paper are the longitudinal and lateral accelerations, the yaw rate (from on-board sensors); the longitudinal velocity (from the odometer); the GPS position, heading angle and velocity; the gas pedal position and the brake cylinder pressure (see [7, Table 2]). Data logged at the rate of 0.05 s are used in this paper.

The test route was driven by 24 users twice, with and without the driver support systems. The logs, in total, represent 35 hours

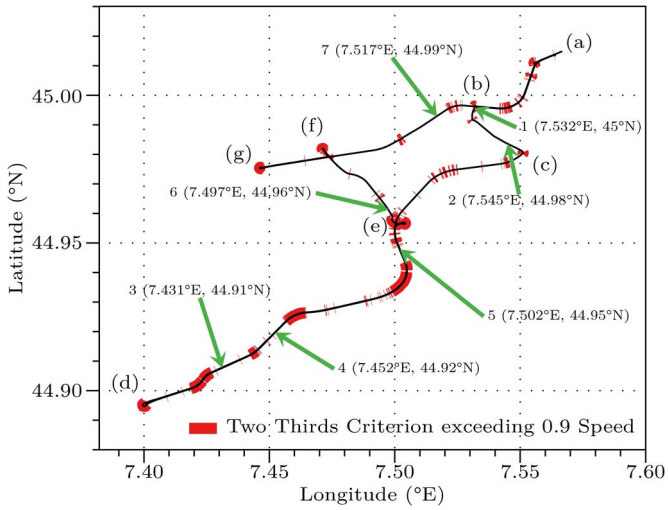

Fig. 5. Test route used for validation. It is located near CRF headquarters in Piemonte region, Italy. Segments marked in red refer to points where, at least for one trial, the speed exceeded 0.9 times the Two-Thirds law limit, with $\alpha = 3.34\ \mathrm{m}^{2/3}/\mathrm{s}$ (0.5 quantiles).

of driving, which means approximately 2.5 million samples per signal.

Beside the raw data fields, a set of computed fields has been derived, including: Cartesian coordinates (x, y, and z), curvilinear abscissa, curvature of the trajectory, and the speed according to the two-thirds law (at 0.5 quantiles). The local curvature has been calculated by fusing lateral acceleration and GPS signals, and represents the actual curvature of the trajectory (not the curvature of the road/lane).

To allow comparisons and aggregation of the 48 trials, a common curvilinear abscissa has been defined. For this—and given the aim of the work— a set of salient landmarks have been identified along the route, where the criterion for "saliency" was the local ratio between speed and the two-thirds power law speed limit. Fig. 5 marks with red the points where at least one driver reached or trespassed the speed of 0.9 times the limit.

According to this preliminary analysis, 7 landmarks have been selected and marked with coordinates on the map. The corresponding points on the track are the beginnings of the interesting segments.

For each landmark and for each trial, data were spline-interpolated and resampled at constant increments of curvilinear abscissa (resulting steps of about 1 m). For each trial, the curvilinear abscissa was then shifted to align the origin to the given landmark.

As a result, charts similar to Fig. 6 were obtained (where the origin of the abscissa corresponds to the landmark). They show the speed profiles of each driver. The thick blue line and the orange lines represent the average speed $\bar{v}(s)$ and the $\bar{v}(s) \pm \sigma_v(s)$ —where $\sigma_v(s)$ is the standard deviation of the speed at the curvilinear abscissa s— respectively. Finally, the thick red line represents the speed limit obtained from (6), using for κ the average curvature $\bar{\kappa}(s)$ of the individual trajectories (thus representing the mean trajectory). Similar charts are found for the other landmarks in Fig. 7. In particular landmarks 3 and 4 are in the motorway. For these, as already noted in [7], the criteria for human speed choice do not match

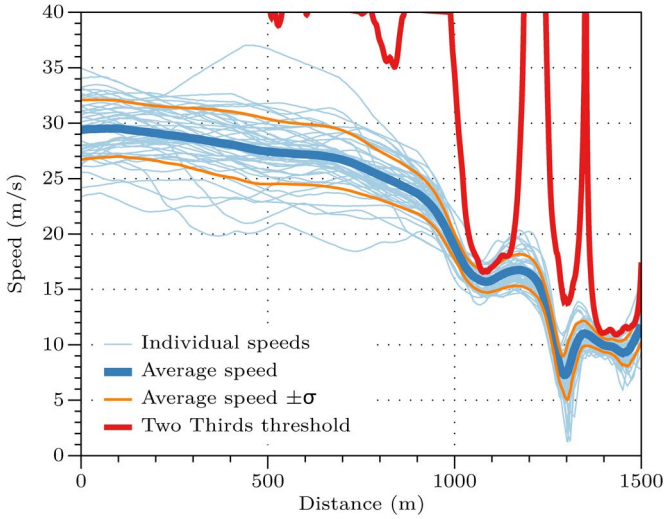

Fig. 6. Speed profiles as functions of the curvilinear abscissa (as distance from landmark), after landmark 5. The two-thirds speed limit ($\alpha = 3.6\ \mathrm{m}^{2/3}/\mathrm{s}$) is shown by the thick red line.

the ordinary roads (for landmark 3 the two-thirds speed limit of the *mean* trajectory is larger than 40 m/s and thus it lays out of frame).

In the following we will focus in particular on an extended road stretch encompassing landmarks 5 and 6, shown in Fig. 8. This stretch collects many interesting features: it includes a right bend at the motorway exit ramp (at 1000 m); a junction with yield sign (at 1200 m); a wide U turn (at 1300 m–1400 m), marked with the first yellow band and the yellow circle in the mini map; a low-curvature link (at 1500 m–1800 m); an S-shaped junction with priority rights (at 1900 m–2100 m), marked with the second yellow band and circle; and lastly an extra-urban straight road with a roundabout (at 2800 m), shown by the third yellow mark. The mean trajectory curvature is shown on the upper part of the figure, with an indication of where the accelerator pedal was completely released.

It may be deduced that most speed profiles comply with the two-thirds speed limit. Only occasionally there were few single users that slightly exceeded the limit. However there is an important systematic exception, which happens at the yield sign (at 1200 m). Here all users reduced the speed more than necessary for the curve. In fact they had to give way, and the curvature was not the limiting factor. This situation can be better seen in Fig. 6.

IV. ADAS Applications

A. Curve Warning Systems

For driver assistance applications, the curve behavior may be used as a *reference maneuver*. For instance, to compare the actual human driver control $j^*(t)$ to the control $j(t)$ that ought to be used, as reported in [38]. However, a simplified method—with no need for estimating the real longitudinal jerk $j^*(t)$—may focus only on $j(0)$, considered as the control input that is *immediately necessary* to negotiate the curve, and raise a warning when it is unlikely to be produced by the human driver. This latter method is hereafter described.

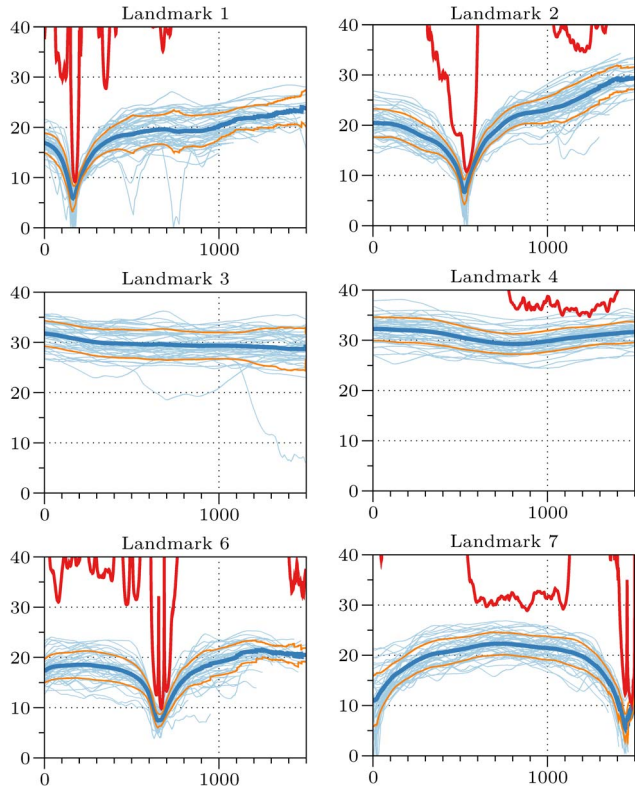

Fig. 7. Details for speed profiles after landmarks 1–4 and 6–7. Axes ranges and legend—omitted for compactness—are as for Fig. 6. Note: For landmark 3, the average two-thirds law speed limit is out of frame.

1) Detection of Maneuvers that Cannot be Human-Directed: The condition:

$$j(0) \leq j_{th} \tag{24}$$

is used to discriminate maneuvers that cannot be human-directed.

To set a proper value for the threshold(s) j_{th}, the data set given in Section III has been studied. Fig. 9 summarizes the main findings. The left part of the figure shows the distribution of acceleration adjustments (current acceleration minus initial acceleration) that follow a sudden and complete release of the gas pedal of at least 10% of the full pedal stroke. There are 3442 such events in the logs: 1 every 36 seconds on average. These events represent all human actions directed to reduce the acceleration, not necessarily related to curves. In the whole, they give a picture of the adjustments that can be produced by a human driver acting on the gas pedal. The median and the 0.01 quantile curves are also shown in the chart. The slope of the lower quantile curve corresponds, approximately, to $-1.5\ \mathrm{m/s}^3$. Thus, 99% of human actions on the gas pedal produce a longitudinal jerk above $-1.5\ \mathrm{m/s}^3$. The right part of Fig. 9 is similar, except that it represents actions on the brake pedal—i.e., sudden brake press from zero. There are 1530 such events in the logs. Brake actions are more effective: the 0.01 quantile corresponds to approximately $-5\ \mathrm{m/s}^3$, being the median jerk $-1.5\ \mathrm{m/s}^3$.

2) Advisory and Cautionary Warnings: Preventive safety system often categorizes two levels of warning: advisory

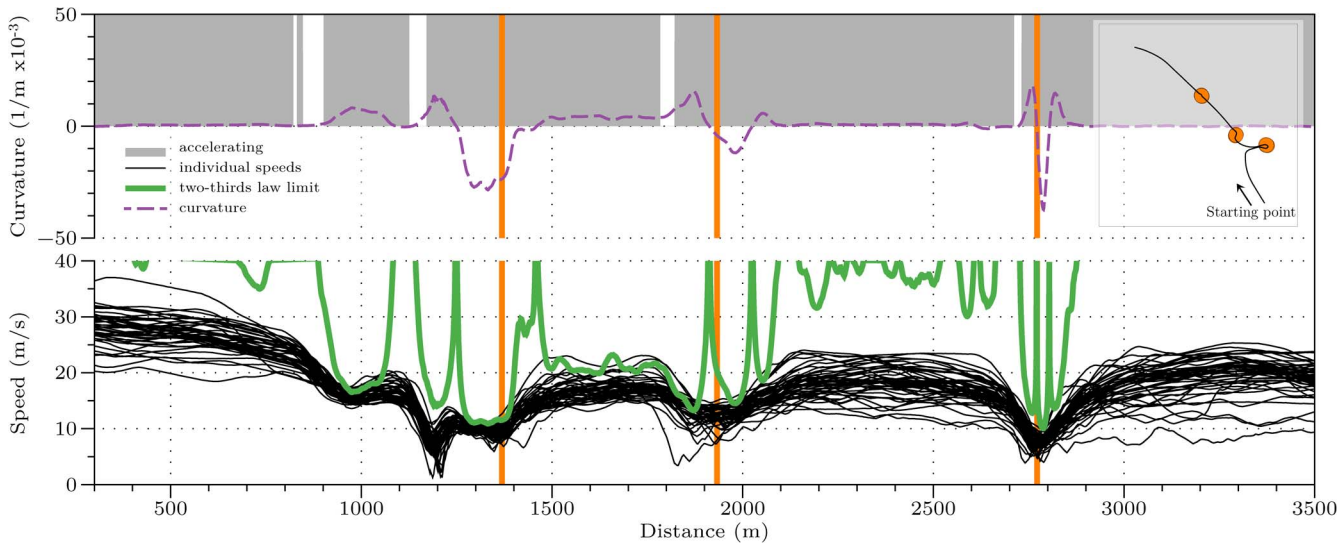

Fig. 8. Extended range after landmark 5, also showing individual values for the speed limit, filtered curvature, and ranges where at least one driver is accelerating (gray background). The inset at top left represents the local trajectory, with orange circles corresponding to curves at the curvilinear abscissae marked by vertical orange lines in the main chart.

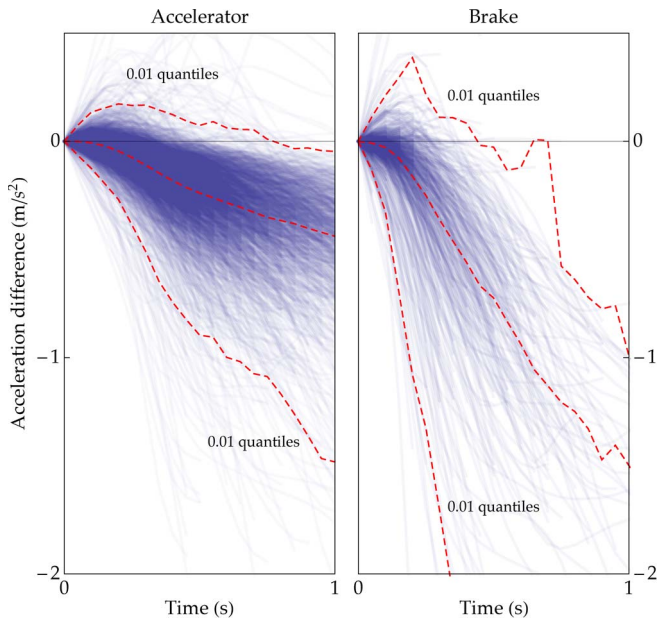

Fig. 9. Envelopes of human longitudinal control.

(usually yellow coded) and cautionary (red). These can be easily implemented by computing two behaviors for each curve, with different settings for the curve speed limit.

For instance, for the advisory warning one might adopt the 99.9 percentile ($\alpha = 3.7$ m$^{2/3}$/s) in (3) with $j_{th} = -1.5$ m/s^3 (0.01 quantiles), which means that a yellow warning is produced when there is only 0.01 probability to comply with the 99.9 percentile of the curve speed model, if acting only on the accelerator. In practical terms, it means that without braking the speed in the curve will exceed what any human would like. In [38] similar settings ($j_{th} = -2.0$ m/s^3) are assumed, but the curve speed model was (4).

For cautionary warning, a larger speed—but still within the friction ellipse—may be set in the curve. For example, in [38] cautionary warning is produced with curve speed 1.2 times the speed used for advisory warning. This time, the threshold may be chosen with respect to the median brake curve, i.e., $j_{th} = -1.5$ m/s^3 (so to leave a margin for maneuvering). In practical terms, this means that the maximum human accepted speed in curve is going to exceed by 20%, unless the driver brakes more than the average.

3) System Performance: An example of how the system works in the real life with said settings is here given. Fig. 10 compares two cases, in which a warning was observed at landmark 1, with the two fastest cases without warnings. The initial speed was even faster for the latter two, but the drivers implemented smooth deceleration in advance by themselves. Conversely, the drivers of the former two cases did not reduce the speed, until the warning happened. The brake maneuver that followed was thus more intense, peaking at approximately -5 m/s^3 instead of the -2.5 m/s^3 of the no-warning cases (Fig. 10, top). The curve speed was obeyed in the no-warning cases, but was undershot with the warnings. In the worst case, the warning (represented by shaded vertical band) was produced approximately 70 m to 80 m (or 3.7 s to 4.2 s) before the curve.

B. Speed Control

For automated speed control, the curve behavior can be used to generate a target maneuver for tracking. The maneuver, which is available as a symbolic function of time (the polynomial coefficients returned by the algorithm in Section II-E), can be updated within a receding horizon scheme.

It has to be noted that this scheme has some similarity with human optimal feedback control (OFC) [29], [40], with which it shares desirable features, such as the fact that the update rate may be slower than the tracking rate, and that only task-relevant deviations occurring between updates are corrected (minimum intervention principle) [30], [41].

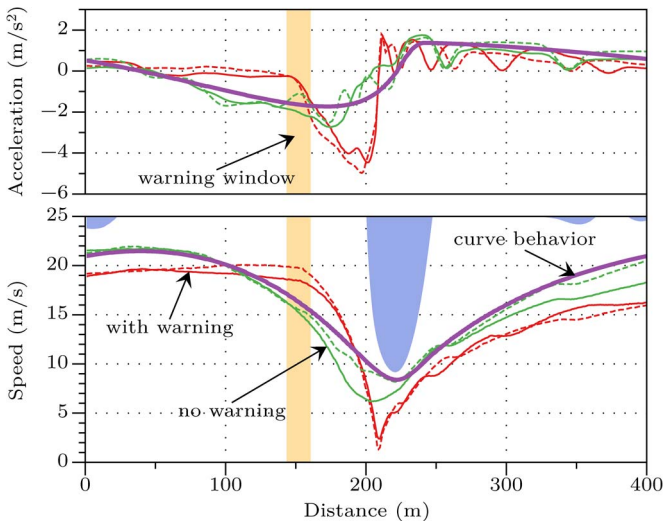

Fig. 10. Example of assistance by the system at landmark 1: green curves are the two fastest cases with no warnings, red are two cases where warnings were raised, and the thick purple line represents the artificial curve behavior.

Of course, for automated driving, the computation of curve speed must be made using a speed limit smaller than that for warning: for example, 5 percentiles of human speed choice ($\alpha = 3.06$ m$^{2/3}$/s) in (3).

The thick purple line in Fig. 10 shows the artificial curve behavior generated with the above criterion using OFC (i.e., continuous update of the target plan). The initial conditions were set to match one of the green curves ($v_0 = 21$ m/s, $a_0 = 0.5$ m/s^2). The minimum time weight was set to $w_T = 1$ m^2/s^6. This value is chosen to match one of the green curves and is maintained for the interval, in which actions on pedals were recorded, i.e., until $x = 230$ m. After this point it is reduced to $w_T = 0.04$ m^2/s^6. The desired free-flow speed was set equal to the maximum speed of the green curve ($v_d = 22$ m/s). With these settings one of the green curves (i.e., a case without warning) is reproduced.

Fig. 11 shows the speed profile that is produced for the long stretch from landmark 5 to 6. The desired speed v_d is set at 28 m/s in the motorway exit ramp (until the yield sign at approximately 1200 m abscissa), then it is set at 18 m/s. These values are deduced from the uniform speed parts that can be observed in the records. The time weight is set to 0.4 m^2/s^6 for the exit ramp, and to 0.1 m^2/s^6 for the rest.

Note that the artificial behavior mimics the average driver behavior with some exception: firstly, it does not reduce the speed at the yield sign—but it was not designed for this; secondly, it tends to be more consistent in passing the curves at their prescribed speed, albeit this speed slightly mismatch the human choice in some case.

C. Rationale for the Selection of w_T and v_d

The above motor primitives include two parameters, v_d and w_T, which model *motivation* states. In general terms, the parameter v_d describes the aimed speed in free-flow (it also exists in many other driver models), while w_T represents how aggressive the artificial driver is—thus describing the tradeoff between smoothness and speed. In fact, w_T determines when the curve primitive is selected over the free-flow, and thus how much the driver waits before initiating a brake maneuver (Fig. 4). When speeding up, w_T also determines how quickly the desired speed is regained. In a subsumption architecture, these two parameters are set by a higher level of the architecture that instantiates the primitives [38]. More than one primitive per type might be instantiated for evaluating alternative options—i.e., to discover what the actual driver's motivations may be—and they remain covert until one is eventually selected. Moreover, in different situations, and in particular for primitives of different type (e.g., brake vs. speed up), different w_T may be used. This is analogous to real human drivers, who sometimes are more aggressive, sometimes less, and are definitely jerkier when using the brake (Fig. 9).

If the motor primitives are used to mirror the human driver, as for an assistive applications, there is little need to mirror the free-flow primitive, and thus to guess v_d exactly. It can be assumed that the initial jerk for free-flow will be close or greater than zero, at least if the driver is marching below or close to the desired speed. The main focus in assistive application is rather put in evaluating the control necessary to negotiate a curve, and in particular detecting when it trespass the critical threshold. One can assume an average driver (say $w_T = 0.2$ m^2/s^6 to 0.4 m^2/s^6) to obtain an estimation of the moment, in which the driver begins to brake. For example, at the exit of the motorway (Fig. 11) the first deceleration begins at about 650 m and ends at about 950 m, which is matched by $w_T = 0.4$ m^2/s^6. If w_T were set to say 0.1 m^2/s^6, the brake would begin 180 m before. Nonetheless, estimating when the brake maneuver begins is still not so important: the important thing is estimating when the threshold is trespassed. Indeed, close to the curve and to the threshold, the needed control is little influenced by w_T, and even a simple minimum jerk criterion ($w_T = 0$) can prove sufficient for detecting critical states. For example, for the fastest maneuver shown in Fig. 10, the jerk threshold would be trespassed only 4 m in advance if using $w_T = 0.1$ m^2/s^6 rather than $w_T = 1$ m^2/s^6.

If the motor primitives are used for automation, v_d and w_T take the meaning of target speed and aggressiveness of designed automation. In this case, v_d should be set by some layer at strategic level (e.g., derived from legal speed limits). Conversely w_T must be acceptable to the human guest, which means that, since the mirroring process is taking place in the reverse way (the human mirroring the artificial driver), the human must interpret automated maneuvers as if they were done by a correct driver. Any w_T within the range of real human drivers may be acceptable—albeit the human guest might perceive that the automated vehicle is very conservative or very aggressive if we chose extreme values for w_T. As an example, the choice of $w_T = 0.1$ m^2/s^6 for both brake and acceleration, drives in the middle of the distribution of human drivers in Fig. 11 in the non-motorway section, but it would be probably better to chose $w_T = 0.4$ m^2/s^6 for braking not only for the motorway exit. In Fig. 10 the selected w_T values are those that best fit the fastest brake observed behavior ($w_T = 1$ m^2/s^6 and $w_T = 0.04$ m^2/s^6 for slow down and speed up, respectively). Note also that the choice $w_T = 0.4$ m^2/s^6 for

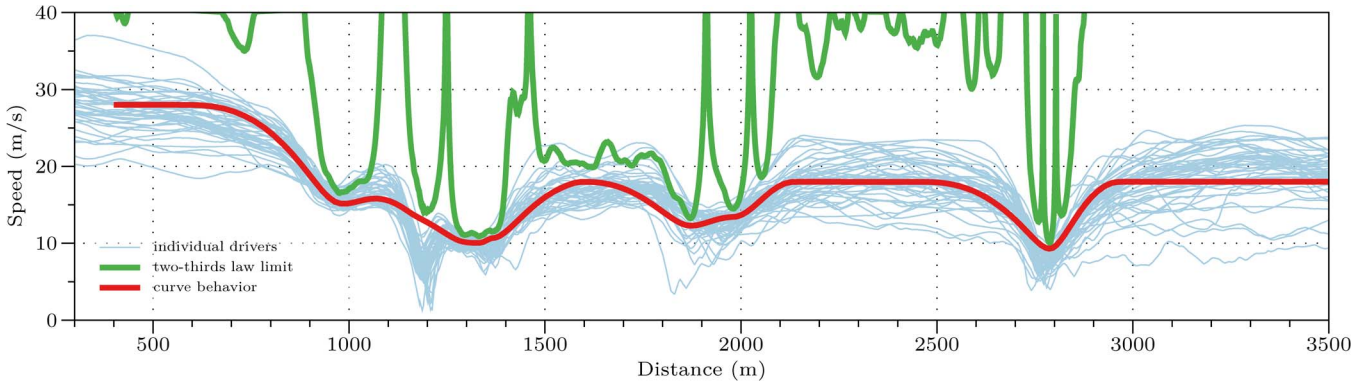

Fig. 11. Same extended range after landmark 5 as reported in Fig. 8, where the speed profile produced by the subsumptive architecture for automated speed control is also reported.

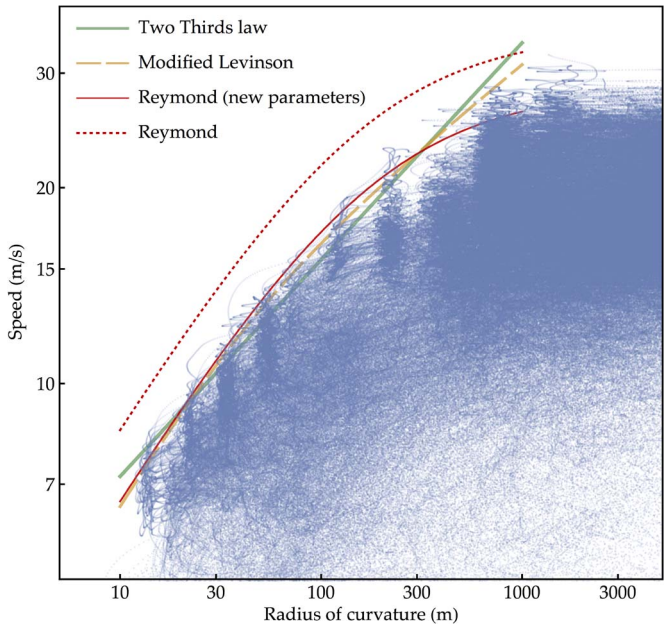

Fig. 12. Comparison of curve speed choice models to the experimental data set.

brake and $w_T = 0.1$ m^2/s^6 for acceleration, would still fall inside the envelope of the observations.

V. Comparison of Human Speed Choice Models

As discussed in Section II-B, the speed selected in curves by human drivers is the foundation of any curve driver assistance system. As noted for Fig. 11, a mismatch between the human speed choice and the model may cause the artificial system to depart from the average human driver behavior.

Fig. 12 compares the three models in Section II-B with the curvature–speed couples observed in the experiment of Section III. The chart shows only data related to the non-motorway part of the test circuit (approximately 1.5 million points). Motorways have been excluded because of the reasons already mentioned above and in [7]. The observed speed-curvature couples form denser clusters of points corresponding to the main curves in the circuit.

The tips of these clouds are approximately aligned with a straight line with a slope that is well fitted by the two-thirds law (3). The modified Levison's fit (4) seems to capture a slight deviation from straightness.

The largest cluster is at the top right, with speed in the range 15 m/s to 25 m/s and radius of curvature larger than about 800 m. These are large curves and straight segments, which occur most of the time (Fig. 5). However, it should be noted that the legal speed limit restricts observed speeds to a maximum of 25 m/s, i.e., 90 km/h. Therefore, comparison with models is restricted to the region where the speed chosen by human drivers falls below the legal speed limit, and the curves of the models are truncated above the radius of 1000 m. The minimum observed radius, at the opposite side, is about 15 m.

The original parameters of Reymond's model [17] for normal driving ($k_1 = 7.64$ m/s^2 and $k_2 = 6.32 \times 10^{-3}$ m^{-1}) would produce the dotted curve, which clearly overestimates the speed envelope. These parameters were originally derived form experiments on a test track, whereas the data shown here are for real users in real roads. If the parameters are adjusted to better fit the current data, the solid curve is obtained, with $k_1 = 4.58$ m/s^2 and $k_2 = 5.69 \times 10^{-3}$ m^{-1}. The latter curve seems to better cope with the top speed of the rightmost cluster. However, as said above, this speed is presumably the legal speed limit and may not represent the speed a human driver would otherwise chose in very large bends. The literature reports other formulas for fitting the curve speed, which are discussed in [13], or in the original Levison's report [15]. However they would not fit the data as well, or would fit the data only over a much narrower radius range.

VI. Conclusion

A bio-inspired curve behavior for autonomous driving has been presented. It is based on optimal motor units, or *motor primitives*, which are then combined into more complex behavior using an action-selection mechanism.

This curve behavior produces human-like maneuvers that can be exploited to implement different levels of automation. For driver assistance, it may be used in a mirroring fashion to spot human incorrect actions. For automated speed control it gives high-level trajectory description for tracking.

One of the most important advantages of the adopted subsumption architecture is scalability: while this paper deals only with curve negotiation, additional motor primitives may be included within the same framework, to extend the functionality.

A detailed description of the implementation of the two motor primitives—curve an free-flow—has been given, and a large experimental data set has been used to validate and tune the developed behavior.

Lastly, one important aspect of curve driving is the human speed choice. For this, the paper introduces speed choice models, highlighting their sensory-motor nature. Three models are compared to the experimental data. To Authors' knowledge, this is the largest dataset ever used for human curve speed validation, encompassing a radius range from 15 to 800 m.

As a future work, within the EU project "adaptIVe," Authors plan to redesign the co-driver of the interactIVe project to also support automation—it was in the origin conceived for mirroring only—by including other longitudinal and lateral motor primitives.

REFERENCES

[1] R. A. Brooks, "A robust layered control system for a mobile robot," *IEEE J. Robot. Autom.*, vol. 2, no. 1, pp. 14–23, Mar. 1986.

[2] T. J. Prescott, P. Redgrave, and K. Gurney, "Layered control architectures in robots and vertebrates," *Adapt. Behav.*, vol. 7, no. 1, pp. 99–127, Jan. 1999.

[3] R. Rice, "Measuring car-driver interaction with the g–g diagram," SAE, Warrendale, PA, USA, Technical Paper 730018, 1973.

[4] Y. Hisaoka, M. Yamamoto, and A. Okada, "Closed-loop analysis of vehicle behavior during braking in a turn," *JSAE Rev.*, vol. 20, no. 4, pp. 537–542, Oct. 1999.

[5] W. Bartlett, O. Masory, and B. Wright, "Driver abilities in closed course testing," SAE, Warrendale, PA, USA, Technical Paper 2000-01-0179, 2000.

[6] F. Biral, M. Da Lio, and E. Bertolazzi, "Combining safety margins and user preferences into a driving criterion for optimal control-based computation of reference maneuvers for an ADAS of the next generation," in *Proc. IEEE Intell. Veh. Symp.*, 2005, pp. 36–41.

[7] P. Bosetti, M. D. Lio, and A. Saroldi, "On the human control of vehicles: An experimental study of acceleration," *Eur. Transp. Res. Rev.*, vol. 6, no. 2, pp. 157–170, Jun. 2014.

[8] F. Jiménez, F. Aparicio, and J. Páez, "Evaluation of in-vehicle dynamic speed assistance in Spain: Algorithm and driver behaviour," *IET Intell. Transp. Syst.*, vol. 2, no. 2, pp. 132–142, Jun. 2008.

[9] F. Jiménez, Y. Liang, and F. Aparicio, "Adapting ISA system warnings to enhance user acceptance," *Accident Anal. Prevention*, vol. 48, pp. 37–48, Sep. 2012.

[10] C. Sentouh, S. Glaser, and S. Mammar, "Advanced vehicle–infrastructure–driver speed profile for road departure accident prevention," *Veh. Syst. Dyn.*, vol. 44, no. S1, pp. 612–623, 2006.

[11] V. Aguiléra, S. Glaser, and A. Von Amim, "An advanced driver speed assistance in curves: Risk function, cooperation modes, system architecture and experimental validation," in *Proc. IEEE Intell. Veh. Symp.*, 2005, pp. 807–812.

[12] S. Glaser, L. Nouveliére, and B. Lusetti, "Speed limitation based on an advanced curve warning system," in *Proc. IEEE Intell. Veh. Symp.*, 2007, pp. 686–691.

[13] A. M. C. Odhams and D. J. Cole, "Models of driver speed choice in curves," in *Proc. 7th Int. Symp. AVEC*, 2004, pp. 1–6.

[14] M. L. Ritchie, W. K. McCoy, and W. L. Welde, "A study of the relation between forward velocity and lateral acceleration in curves during normal driving," *Hum. Factors*, vol. 10, no. 3, pp. 255–258, Jun. 1968.

[15] W. H. Levison *et al.*, "Development of a driver vehicle module for the interactive highway safety design model," Federal Highway Admin., Washington, DC, USA, Tech. Rep. USDOT-FHWA-HRT-08-019, Nov. 2007. [Online]. Available: http://www.fhwa.dot.gov/publications/research/safety/08019/08019.pdf

[16] W. V. Winsum and H. Godthelp, "Speed choice and steering behaviour in curve driving," *Hum. Factors*, vol. 38, no. 3, pp. 434–441, Sep. 1996.

[17] G. Reymond, A. Kemeny, J. Droulez, and A. Berthoz, "Role of lateral acceleration in curve driving: Driver model and experiments on a real vehicle and a driving simulator," *Hum. Factors, J. Hum. Factors Ergonom. Soc.*, vol. 43, no. 3, pp. 483–495, Jun. 2001.

[18] K. DeFazio, D. Wittman, and C. Drury, "Effective vehicle width in self-paced tracking," *Appl. Ergonom.*, vol. 23, no. 6, pp. 382–386, Dec. 1992.

[19] D. Bottoms, "The interaction of driving speed, steering difficulty and lateral tolerance with particular reference to agriculture," *Ergonomics*, vol. 26, no. 2, pp. 123–139, 1983.

[20] T. Flash, Y. Meirovitch, and A. Barliya, "Models of human movement: Trajectory planning and inverse kinematics studies," *Robot. Autonom. Syst.*, vol. 61, no. 4, pp. 330–339, Apr. 2013.

[21] H. Hicheur, S. Vieilledent, M. J. E. Richardson, T. Flash, and A. Berthoz, "Velocity and curvature in human locomotion along complex curved paths: A comparison with hand movements," *Exp. Brain Res.*, vol. 162, no. 2, pp. 145–154, May 2005.

[22] C. M. Harris, "Signal-dependent noise determines motor planning," *Nature*, vol. 394, pp. 780–784, Aug. 1998.

[23] K. Wevers *et al.*, "Integration of driver support systems—The INARTE project," in *Proc. 6th World Congr. Intell. Transp. Syst.*, 1999.

[24] E. Bertolazzi, F. Biral, M. Da Lio, A. Saroldi, and F. Tango, "Supporting drivers in keeping safe speed and safe distance: The SASPENCE subproject within the European framework programme 6 integrating project PReVENT," *IEEE Trans. Intell. Transp. Syst.*, vol. 11, no. 3, pp. 525–538, Sep. 2010.

[25] F. Biral, M. da Lio, R. Lot, and R. Sartori, "An intelligent curve warning system for powered two wheel vehicles," *Eur. Transp. Res. Rev.*, vol. 2, no. 3, pp. 147–156, Dec. 2010.

[26] F. Biral, P. Bosetti, and R. Lot, "Experimental evaluation of a system for assisting motorcyclists to safely ride road bends," *Eur. Transp. Res. Rev.*, vol. 6, no. 4, pp. 411–423, Dec. 2014.

[27] B. Lusetti, L. Nouveliére, S. Glaser, and S. Mammar, "Experimental strategy for a system based curve warning system for a safe governed speed of a vehicle," in *Proc. IEEE Intell. Veh. Symp.*, 2008, pp. 660–665.

[28] D. Zhang, Q. Xiao, J. Wang, and K. Li, "Driver curve speed model and its application to ACC speed control in curved roads," *Int. J. Autom. Technol.*, vol. 14, no. 2, pp. 241–247, Apr. 2013.

[29] E. Todorov, "Optimality principles in sensorimotor control," *Nat. Neurosci.*, vol. 7, no. 9, pp. 907–915, Sep. 2004.

[30] D. Liu andE. Todorov, "Evidence for the flexible sensorimotor strategies predicted by optimal feedback control," *J. Neurosci.*, vol. 27, no. 35, pp. 9354–9368, Aug. 2007.

[31] A. J. Nagengast, D. A. Braun, and D. M. Wolpert, "Optimal control predicts human performance on objects with internal degrees of freedom," *PLoS Comput. Biol.*, vol. 5, no. 6, Jun. 2009, Art. ID. e1000419.

[32] D. Kim, C. Jang, and F. Park, "Kinematic feedback control laws for generating natural arm movements," *Bioinspiration Biomimetics*, vol. 9, no. 1, Mar. 2014, Art. ID. 016002.

[33] F. Mussa-Ivaldi and S. Solla, "Neural primitives for motion control," *IEEE J. Ocean. Eng.*, vol. 29, no. 3, pp. 640–650, Jul. 2004.

[34] T. Flash and B. Hochner, "Motor primitives in vertebrates and invertebrates," *Current Opinion Neurobiol.*, vol. 15, no. 6, pp. 660–666, Dec. 2005.

[35] M. A. Jenkins and J. F. Traub, "A three-stage algorithm for real polynomials using quadratic iteration," *SIAM J. Numer. Anal.*, vol. 7, no. 4, pp. 545–566, 1970.

[36] P. Cisek, "Cortical mechanisms of action selection: The affordance competition hypothesis," *Philos. Trans. R. Soc. Lond B Biol. Sci.*, vol. 362, no. 1485, pp. 1585–1599, Sep. 2007.

[37] P. Redgrave, T. J. Prescott, and K. Gurney, "The basal ganglia: A vertebrate solution to the selection problem?," *Neuroscience*, vol. 89, no. 4, pp. 1009–1023, 1999.

[38] M. Da Lio *et al.*, "Artificial co-drivers as a universal enabling technology for future intelligent vehicles and transportation systems," *IEEE Trans. Intell. Transp. Syst.*, vol. 16, no. 1, pp. 244–263, 2014.

[39] "interactIVe—Accident avoidance by intervention for intelligent vehicles." [Online]. Available: http://www.interactive-ip.eu/

[40] S. H. Scott, "The computational and neural basis of voluntary motor control and planning," *Trends Cogn. Sci.*, vol. 16, no. 11, pp. 541–549, Nov. 2012.

[41] E. Todorov and M. I. Jordan, "A minimal intervention principle for coordinated movement," *Adv. Neur. Inf. Process. Syst.*, vol. 15, pp. 27–34, 2003.

Paolo Bosetti received the Laurea degree in materials engineering and the Ph.D. degree in materials and structural engineering from the University of Trento, Trento, Italy, in 1997 and 2002, respectively. He is currently an Assistant Professor with the Department of Industrial Engineering, University of Trento, where he is in charge of the courses on manufacturing automation, manufacturing process design, and design of manufacturing systems. His research interests include mechatronic systems, automation, and smart manufacturing systems.

Mauro Da Lio received the Laurea degree in mechanical engineering from the University of Padova, Padova, Italy, in 1986. He is currently a Full Professor of mechanical systems with the University of Trento, Trento, Italy. He was with an offshore oil research company in underwater robotics (EUREKA project). He has been involved in several EU framework programme 6 and 7 projects (PReVENT, SAFERIDER, interactIVe, VERITAS, adaptIVe, and NoTremor). His earlier research activity was on modeling, simulation, and optimal control of mechanical multibody systems, particularly vehicle and spacecraft dynamics. More recently, his focus has shifted to the modeling of human sensory–motor control, particularly drivers and motor-impaired people.

Andrea Saroldi received the Laurea degree in physics from the University of Turin, Turin, Italy, in 1985. Since 1986, he has been with Centro Ricerche Fiat, Orbassano, Italy, as part of a group involved with advanced driver assistance systems. He has been the Project Leader for subproject SASPENCE of the PReVENT Integrating Project and for subproject SECONDS of the interactIVe Integrated Project. His research interests are in processing of sensor data and development of driver assistance functions for preventive safety.